ISSN 1345-3041

Sep.2022 / Vol.179

Mitsubishi Electric

ADVANCE

Power Devices

MITSUBISHI ELECTRIC
Changes for the Better

Sep. 2022 / Vol. 179

Mitsubishi Electric

ADVANCE

Power Devices

• **Editorial Inquiries**

Hideyuki Ichiyama
Corporate Productivity Engineering & Logistics Dept.
Fax: +81-3-3218-2465

Mitsubishi Electric Advance is published on line quarterly (in March, June, September, and December) by Mitsubishi Electric Corporation.

CONTENTS

Technical Reports

Precis
Mitsubishi Electric's power modules, which employ the latest chip and package technology, realize ideal power electronics systems thanks to their high quality, low loss, and excellent noise performance.

Overview

Author: *Shinichi Nishizawa**

Power Devices for a Carbon-neutral Society

Satisfying the rapidly increasing global demand for energy while attaining a carbon-neutral society as proposed by the Conference of the Parties 21 (COP21) and Sustainable Development Goals (SDGs) is an urgent task. One main goal of the UN's SDGs is to solve the energy problem. With electricity accounting for an increasing share of energy demand, it is crucial to develop technologies for using electric power efficiently in order to achieve a carbon-neutral society. This growth in electric power and electronics is being driven by the accelerating trend toward e-mobility, renewable energy, Society 5.0 (Internet of Things (IoT), AI, and network-connected society), and so forth. Accordingly, the Japanese government designated electrification and the use of renewable energy for electric power generation as important technical developments under its "Green Growth Strategy Through Achieving Carbon Neutrality in 2050" issued in 2020. Power devices and power electronics, which control electric power, the flow of energy, and energy utilization, are key components of environmental measures and industrial competitiveness.

New power device technologies having enhanced performance have been introduced from time to time. Examples include: the planar type, trench type, and super junction (SJ) type for metal-oxide-semiconductor field-effect transistors (MOSFETs), depending on the withstanding voltage; and the carrier storage and field stop (FS) structure for insulated gate bipolar transistors (IGBTs). Ground-breaking technical development has pushed their performance for switching devices to the limit. Next-generation power devices are being developed that use new semiconductor materials such as silicon carbide (SiC) to overcome the physical limits of conventional silicon. In addition, next-generation power devices and power modules are under development by applying a new scaling law to silicon IGBTs while combining complementary MOS (CMOS) digital technologies. These next-generation higher-performance power devices and power modules offer new functions and values. Till now, the main role of power devices has been to control the output to ensure that the equipment in which they have been installed operates in an optimum way. Combining digital technologies with this output control enables self-examination and self-restoration of power devices, other modules, and equipment, and allows them to cooperate with the input side, for example, linkage with higher-order equipment and other units via networks. Thus, for new intelligent power devices, power devices and CMOS digital technologies are being combined in a cooperative way: they function as complex systems that have communication, digital, AI, and IoT functions, in addition to improved conventional single functions such as higher energy-saving performance of electric power converters. On the new energy grids where cyberspace converges with physical space, namely the flow of information and the flow of energy, power devices and power electronics equipment themselves function as virtual systems that cooperate and link with each other to optimize the efficiency of electric energy in society as a whole.

**Professor, Research Institute for Applied Mechanics, Kyushu University*

Under such circumstances, a new index that indicates the energy-saving effect of power devices and power electronics and also their spread, the “negawatt cost,” has been proposed. In terms of negawatt cost, the energy-saving effects brought about by power devices and power electronics are regarded as the same as renewable energy power generation effects, because the saved energy can be effectively used for other purposes, and the energy-saving cost is equal to the power generation cost. The index comprehensively evaluates technologies that support a carbon-neutral society in 2050 by bridging the divide between energy-saving and new energy.

In June 2021, the Japanese Ministry of Economy, Trade and Industry positioned the digital industry, digital infrastructure, and semiconductors as principal national items in its Strategy for Semiconductors and the Digital Industry, and stated that it would actively strengthen them. The government announced that it would promote advanced logic semiconductor design, for example, a post-5th Generation Mobile Communication System (5G), application system base semiconductors, and edge AI chips/next-generation computing. Meanwhile, as measures to promote green innovation of semiconductor technologies, the government is focusing on shifting to power semiconductors, optoelectronics devices (information electronics), and photoelectric fusion. These are key materials for saving energy and reducing electric power consumption to cope with the increasing use of electricity as society digitalizes. Power devices, which are crucial for this digital transformation, are themselves evolving into new intelligent power devices in combination with digital technologies and will control the carbon-neutral society.

Amid these drastic changes, I sincerely hope that Japan remains ahead of others through cooperation between industry and academia.

SiC Power Module for Automotive

Authors: *Hideo Komo** and *Shoichi Orita**

1. Introduction

In recent years, in order to reduce greenhouse gas emissions, governments around the world have been actively promoting vehicle electrification. From 2025, sales of gasoline-fueled automobiles will be gradually restricted and thus sales of new electric-powered automobiles are expected to increase.

Mitsubishi Electric Corporation released small, highly-reliable T-PMs in 2001 and the J1 Series case-type automotive power module in 2015, contributing to vehicle electrification by supplying Si power devices (Fig. 1). To encourage the spread of xEVs in the future, the cruising distance of automobiles needs to be increased. One way of doing this is to reduce the loss in inverters. The loss in semiconductor devices for SiC power devices is approximately 70% smaller than that for Si power devices. Therefore, SiC power devices are being developed as next-generation semiconductor devices to reduce the loss in inverters.

Mitsubishi Electric is developing SiC T-PM (provisional name) by combining its accumulated know-how on SiC power devices and T-PM packages. This paper introduces emerging issues in the development and countermeasures.

2. SiC T-PM

2.1 SiC power devices(1)

Mitsubishi Electric started developing SiC power devices in the 1990s and in 2010, released power modules for electric railways that included first-generation SiC metal-oxide-semiconductor field-effect transistors (MOSFETs). In 2013, we started mass-producing the second-generation devices with optimized cell size and injection conditions, and have been supplying them for use in consumer goods, industry, and automobiles. Currently, we are developing the trench type as the third generation (Fig. 2).

Technological issues of the trench structure include the degradation of gate insulators due to high electric field and limitations on reducing the on-resistance (Ron) due to densification. To solve these issues, the third-generation trench-type SiC power device (multiple ion-implantation into tilted trench sidewall metal oxide semiconductors (MIT2-MOSs)) currently being developed uses an electric field relaxation structure and n+ JFET doping (JD) (n layer) formation, which are our proprietary technologies.

The gate insulator may deteriorate and the device may become damaged by the high electric field that occurs at the corner of the trench gate. To prevent these problems, a p+ bottom P-well (BPW) is provided at the bottom of the trench gate to protect the gate oxide from the high electric field that occurs when a current is carried, thus enhancing the reliability. At this time, electric charge accumulation up on the BPW may hinder high-speed operation and thus increase the switching (SW) loss. To avoid this, a p sidewall connection (SC) is provided to allow the BPW to have electrical continuity with the p layer and source electrode. This stabilizes the electric potential of the BPW and encourages the discharge of electric charges accumulated on the BPW, reducing the SW loss.

Fig. 1 Automotive Si power module

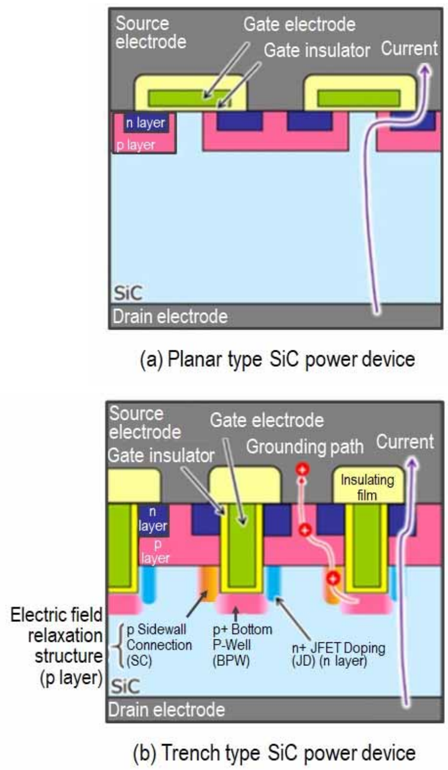

Fig. 2 Schematic diagrams of Mitsubishi Electric SiC MOSFET

*Power Device Works

For the trench gate structure, Ron was reduced through densification. However, there was a limit on reducing Ron because the drain current density increases as a result of densification. To solve this, JD (n layer) is provided on the side of the trench gate to increase the density of carriers on the drain current path and reduce Ron.

Compared to the planar type, on MIT2-MOSs, Ron was reduced though densification of carriers and the trade-off curve between Ron and gate threshold voltage (Vth) was also improved. Thanks to this improvement, the standardized on-resistance of MIT2-MOSs with high-withstand-voltage devices (rating of 1,200 V) (avalanche voltage of 1,500 V) is 1.9 mΩ·cm^2 at room temperature when Vth is 4.1 V.[2]

2.2 T-PM packages[3]

Previously, Mitsubishi Electric released DIPIPM for consumer goods. We applied the package technologies used for DIPIPM to T-PM to create a small, low-profile, highly-reliable transfer molded product for automotive applications.

One characteristic of this product is that the thermal cycle reliability is higher than that of case-type modules, which was achieved by matching the coefficients of thermal expansion (CTE) of the chips and the molding sealing resin. In addition, the electric connection with chips was changed from wire bonding to direct lead bonding (DLB), which allows the power cycle reliability to be retained longer and reduces the interconnection resistance and self-inductance.

Regarding the cooling structure of the chip, thick copper (heat spreader) is provided immediately below the chip, and an insulation sheet that has higher thermal conductivity than the molding sealing resin is provided below that. While the electric insulation performance remains high, the heat from the chip is spread by the heat spreader and passes through the insulation sheet. This structure reduces the steady thermal resistance and also transient thermal resistance, which is important for automotive applications.

The output of 2-in-1 T-PMs can be changed by changing the number of devices connected in parallel depending on the application, like discrete devices, and thus the circuit can be configured flexibly. Figure 3 illustrates the structure of a typical case-type module and T-PM package.

2.3 SiC T-PMs

By combining our accumulated SiC power device technologies with the high-reliability, low-inductance characteristics of T-PMs, we have achieved the low loss that is required for SiC power modules, while increasing the output density, reducing the size, and raising the reliability. However, SiC power devices are semiconductor devices that can work at high temperatures at 200°C or higher and at high speed, therefore to make the most of these characteristics, the conventional T-PM packages need to be improved, with increased heat resistance, lower thermal resistance, and lower inductance. Regarding the higher heat resistance and lower thermal resistance, in particular, new elemental technologies need to be developed.

The two main types of materials for which new elemental technologies need to be developed are as follows (Fig. 4).

(1) Chip bonding materials

As chip bonding materials, Mitsubishi Electric has been using mainly an Sn (tin) alloy solder material in accordance with the regulations banning the use of lead. When SiC power devices are mounted on T-PMs, to make the most of the functions of the SiC power devices, a method of use that increases the maximum chip junction temperature is required. However, the thermal resistance of conventional solder materials is not sufficient for the increased junction temperature, which could impair the power cycle reliability.

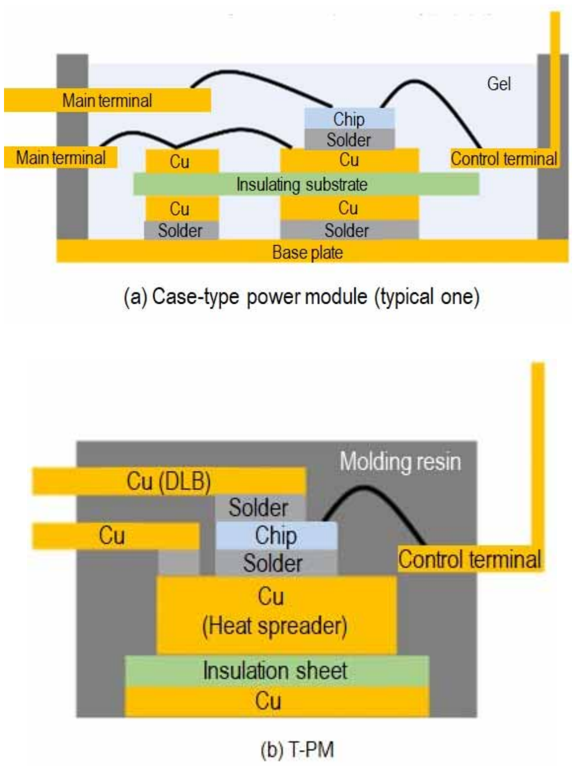

Fig. 3 Representative example of case-type power module and package structure of T-PM

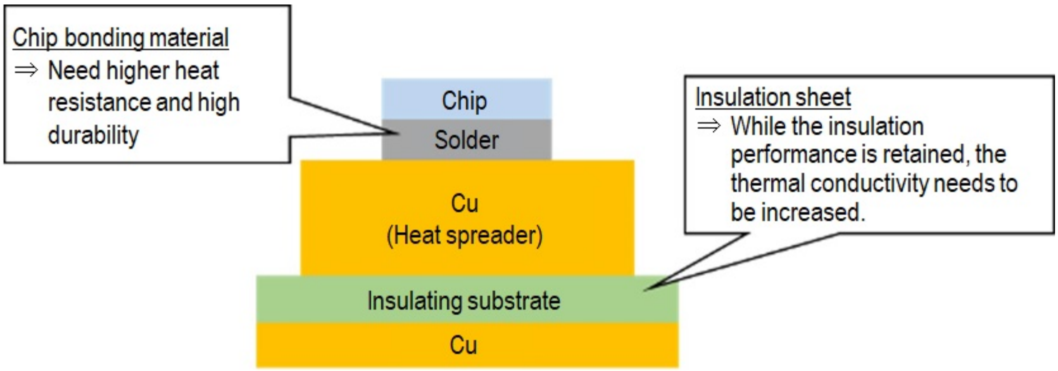

Fig. 4 Material issues of SiC T-PM

(2) Insulation sheets

Mitsubishi Electric has been developing insulation materials to increase the heat dissipation of insulation sheets, improving the thermal conductivity. To cope with the high output density and high junction temperature of SiC power devices, the thermal conductivity needs to be further improved while retaining the insulation performance of insulation sheets.

Chapter 3 describes technological issues with these materials and countermeasures.

3. Technological Issues with SiC T-PMs and Countermeasures

3.1 Chip bonding materials

Generally, to realize high-temperature operation, high-temperature solder in which lead was the main component was adopted. However, restrictions on the use of certain hazardous substances in electrical and electronic equipment under the RoHS Directive have been imposed, and so global efforts are being made to develop lead-free solder that mainly contains tin (Sn).

The solidus temperature of lead-free solder mainly containing tin is 200-250°C. Therefore, even if high-temperature operation is realized by SiC power devices, the durability of the chip joints may be lower. To counter this loss of durability, various types of elements need to be added to the solder. However, doing this reduces the thermal conductivity and SiC power devices may not exert their full performance due to the poorer heat dissipation.

In order to realize both highly durable chip joints and high heat dissipation, a new bonding material is needed. Mitsubishi Electric focused on silver (Ag) sinter bonding. For the Ag sintering material, the phenomenon of reduced melting point is utilized by using Ag particles covered with a thermal-decomposable organic protective coating to realize bonding at 300°C or lower, equivalent to the temperature of solder bonding. Thanks to this, after bonding, the melting point of the bonding material

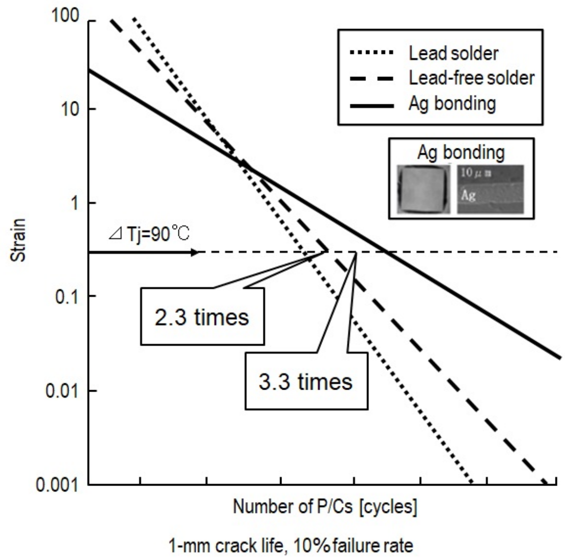

Fig. 5 Stress endurance diagram of various bonding materials

is 900°C or higher and its thermal conductivity is approximately 200 W/m·K.

Figure 5 shows the results of thermal cycle tests (Mitsubishi Electric's proprietary method) of lead solder, lead-free solder, and Ag sintering material assuming power cycle reliability. When the values of the strain that occurred in the thermal cycle tests were converted with reference to those that occurred in a power cycle test (Tjmax = 175°C, ΔTj = 90 K), the overload tolerance of the lead-free solder was 2.3 times that of the lead solder, while the overload tolerance of the Ag sintering material was 3.3 times that of the lead-free solder. These results show that the Ag sintering material is suitable for enhancing the power cycle reliability in high-temperature bonding.

3.2 Insulation sheets[4]

An insulation sheet consisting of a high-thermal conductive ceramic filler (hereinafter “filler”) and resin has heat dissipation and dielectric voltage. The material, shape, filling factor, and other properties of the filler are closely related to the heat dissipation of the insulation sheet. The dielectric voltage sometimes has a trade-off relationship with the heat dissipation. Accordingly, although the heat dissipation can be improved by adjusting the filler, it may be difficult to secure the dielectric voltage. Thus, insulation sheets need to be designed such that the heat dissipation and dielectric voltage are well balanced by optimizing various elements (Fig. 6).

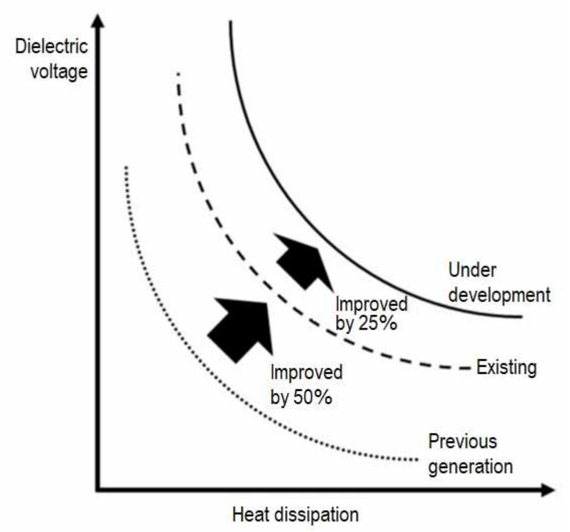

Fig. 6 voltage of insulation sheet

4. Future Application of Automotive Power Modules

The xEV market is rapidly expanding and small- to large-size automobiles are becoming electric-powered. This is generating various needs for power modules. Mitsubishi Electric will continue to develop power module products with reverse conducting insulated gate bipolar transistors (RC-IGBTs), which may help to downsize inverters, in addition to the high-performance SiC power modules described in this paper. We will develop and apply products that satisfy various needs.

5. Conclusion

Mitsubishi Electric has been developing and releasing automotive power modules for more than two decades, contributing to the spread of xEVs. We will continue such development by drawing on our accumulated technologies and know-how and actively develop and use new devices and package technologies to contribute to the accelerating electrification of vehicles.

References

(1) K. Sugawara, et al.: A Novel Trench SiC-MOSFETs Fabricated by Multiple-Ion-Implantation into Tilted Trench Side Walls (MIT2-MOS), PCIM Europe digital days 2021 (2021)
(2) K. Sugawara, et al.: SiC Trench Metal - Oxide - Semiconductor Field - Effect Transistor with Novel Structure Enabling Lower Losses, Mitsubishi Denki Giho, 96, No.3, 160-163 (2022)
(3) A. Iizuka, et al.: Automotive Power Module "J1 Series", Mitsubishi Denki Giho, 94, No.3, 173-176 (2020)
(4) T. Nishimura, et al.: High Performance Transfer-molded Power Module, Mitsubishi Denki Giho, 84, No.4, 219-223 (2010)

TH-Series: 7th Generation IGBT Modules for High-frequency Switching in Industrial Operation

Authors: *Satoshi Kawabata** and *Hiroki Muraoka**

1. Introduction

Power electronics that can use energy and other resources efficiently and effectively are becoming increasingly important in view of recent environmental trends and the social situation. This paper describes the development of the IGBT module TH-series. Mitsubishi Electric Corporation has already started mass-producing the latest seventh-generation industrial IGBT chips and fine-tuned their properties to provide the IGBT module TH-series with a high-speed switching specification. The TH-series can remarkably improve the efficiency of equipment that requires high-speed switching (fc = 20 kHz or higher). Regarding industrial equipment, the switching frequencies at which power devices are used vary (Fig. 1).

2. Characteristics of the TH-series

2.1 Technologies for the seventh-generation IGBT chips[1]

Mitsubishi Electric's IGBT chips have used the CSTBT structure having an electric charge storage layer (CS layer) since the fifth generation and the seventh-generation IGBT chips also have this structure. For the sixth generation, the pitch of the trench gate was narrowed compared to the fifth generation, which further improved the carrier storage effect. The high performance of the seventh generation was realized through ultrathin wafers, metal oxide semiconductor (MOS) structure, and improved structure of the back side. This time, the trade-off of the conventional seventh-generation IGBT chip was mitigated to create the TH-series chip and boost the efficiency of equipment used at a switching frequency (fc) of 20 kHz or higher.

2.1.1 Features of the TH-series[2]

The saturation voltage (VCEsat) of an IGBT has a trade-off relationship with the turn-off power loss (Eoff) and this is often used as an index of an IGBT's property. The seventh-generation industrial IGBT T-series is designed with a saturation voltage (VCEsat) of 1.55 V (@IC = rated current, Tvj = 25°C). If the structure or current density is the same, reducing the switching loss unavoidably increases the saturation voltage (Fig. 2). For equipment involving high-speed switching, the ratio of the switching loss is larger than that of the steady loss by the saturation voltage. Therefore, reducing the switching loss may make the equipment far more efficient even at the slight up of saturation voltage. However, there is a limit of the effect of reducing the total loss through the trade-off between saturation voltage and switching loss. The saturation voltage (VCEsat) of the TH-series was determined as 4.35 V (@IC = rated current, Tvj = 25°C) considering the service conditions of various types of equipment (Fig. 3).

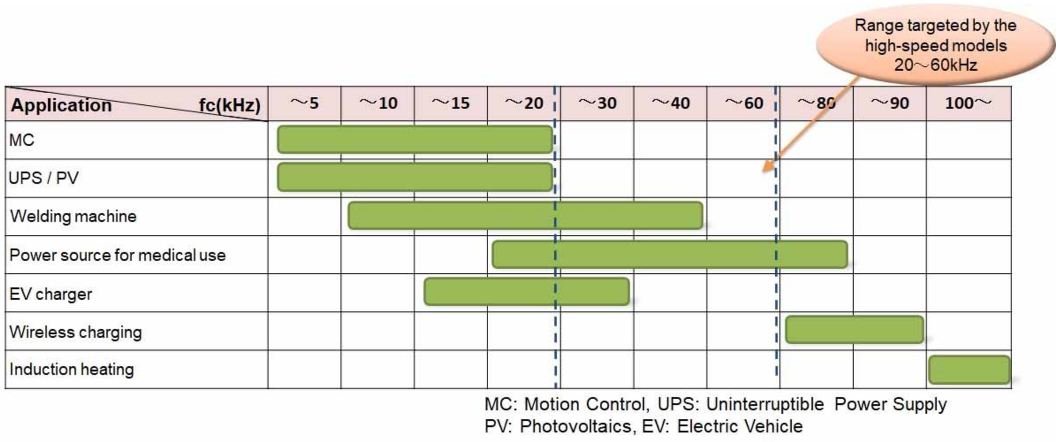

Fig. 1 Switching frequencies for industrial equipment

*Power Device Works

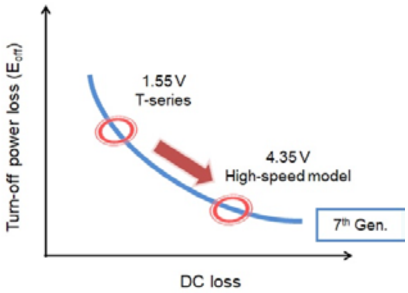

Fig. 2 IGBT trade-off

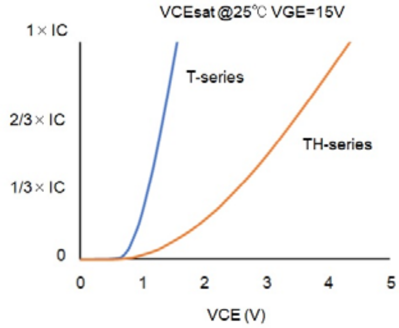

Fig. 3 Static characteristics of T-series and TH-series

The trade-off is adjusted by radiation of life time killers, but this adversely affects the breakdown endurance. Accordingly, this method can be applied only to equipment where it is important to reduce the switching loss at the cost of breakdown endurance and saturation voltage.

As described previously, adjusting and changing the target trade-off between turn-off loss and saturation voltage using life time killers can increase the efficiency of the equipment. However, there is turn-on power loss as a switching loss of IGBTs, in addition to turn-off power loss. Turn-on correlates with VGE(th) and thus reducing VGE(th) can reduce the turn-on power loss. However, equipment involving high-frequency switching may be more affected by noise. Considering the risk of malfunction and device destruction by noise as a result of merely reducing VGE(th), the chips' parasitic capacitance and built-in Rg of the TH-series were optimized accordingly, as is the case with the T-series.

In addition, regarding the high-speed switching specification, adjusting the free wheeling diodes (FWDs) included in the modules may work to reduce the loss, in addition to IGBTs. For diodes, saturation voltage (VF) has a trade-off relationship with the switching loss (Err) like turn-off of IGBTs. Accordingly, the target was changed as well.

As described above, the switching loss of the TH-series was reduced by changing the chip's target based on the T-series. Figure 4 compares the switching waveforms of the T-series and TH-series.

Table 1 lists the main properties of the seventh-generation industrial IGBT module T-series and TH-series for comparison.

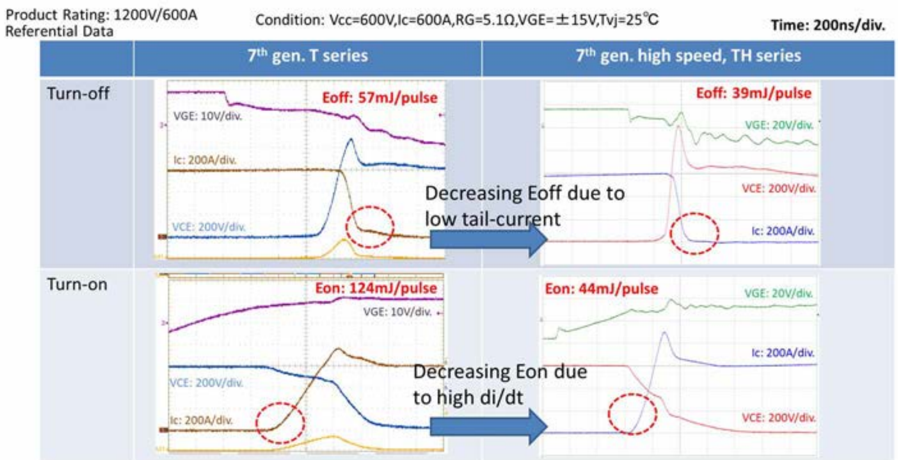

Fig. 4 Switching behavior comparison

Table 1 Comparison data (1200V/600A)

Item	Seventh-generation T-series	Seventh-generation high-speed TH-series*1
Type name	CM600DY-24T	CM600DU-24TH
V_{isol}	AC 4.0 kV	AC 4.0 kV
T_{vjmax}	175 °C	175 °C
Q_G	3700 nC	1500 nC
$V_{GE(th)}$ (typ)	6.00 V	6.00 V
V_{CEsat} (typ)	1.55 V	4.35 V
V_{EC} (typ)	1.65 V	2.35 V
E_{off} (typ)	64 mJ	35 mJ
V_{CCmax}	850 V	850 V

Note[1]: No short-circuit guarantee

2.1.2 Contribution of the high-speed switching specification to equipment

The loss of the seventh-generation T-series and TH-series was simulated to assess to what degree the high-speed specification could contribute to actual equipment. Figure 5 shows the comparison results. Because the high-speed switching specification targets equipment for which the switching frequency is 20 kHz or higher, 30 kHz was used for the calculation. The results show that the switching loss accounted for a large proportion for the T-series, but that it was remarkably reduced for the TH-series. Although the saturation voltage DC loss was increased as a result of reducing the switching loss, the total loss of the IGBT was reduced (Fig. 5).

Even when the switching frequency is increased, the DC loss is the same. Accordingly, the loss of the T-series may be increased at high-frequency operation compared to the TH-series because the switching loss of the T-series accounts for a large proportion (Fig. 6).

When the switching frequency is high, hybrid SiC (silicon carbide) modules and full-SiC modules are options. As an example, the loss of the seventh-generation T-series and TH-series was compared to that of such modules (Fig. 7). Although the TH-series is no match for SiC products as the figure shows, they are suitable for high-speed specifications as Si (silicon) products. We have therefore included them in our lineup as options that users can select.

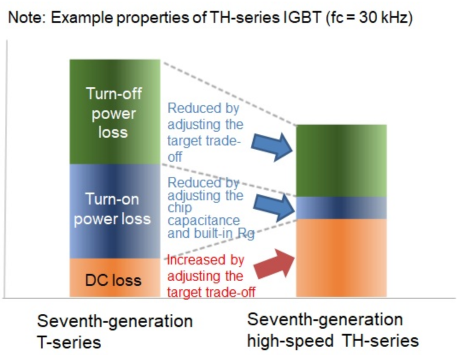

Fig. 5 Comparison for IGBT loss

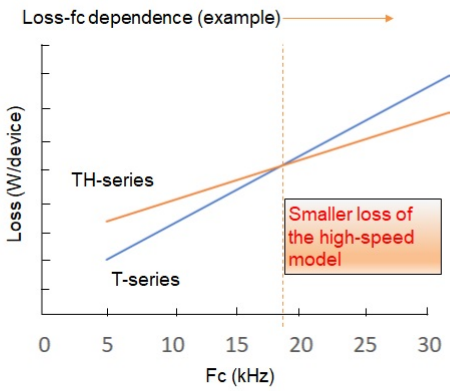

Fig. 6 Loss – fc (per 1 device)

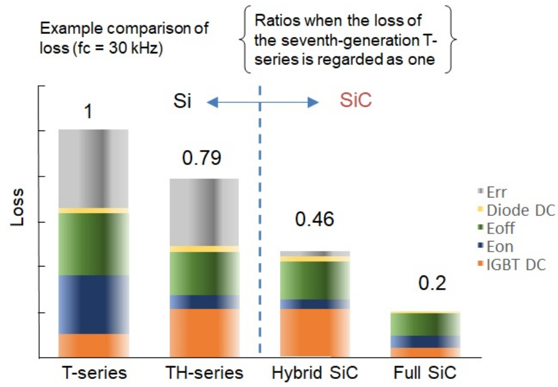

Fig. 7 Loss data for various IGBT modules

2.2 Packaging technologies

The seventh-generation industrial T-series standard type adopted the thick metal substrate (TMS) technology. For the TH-series, ceramic substrates and a copper base structure, which were used for the old generations (up to the six-generation standard type), were used instead of TMS. We focused on ensuring compatibility with our hybrid SiC and securing heat dissipation and thermal capacity because the loss would be considerably large due to high-speed switching (Fig. 8).

2.3 Product lineup

As our product lineup, we offer 1,200 V/200 A, 1,200 V/400 A, and 1,200 V/600 A (all 2-in-1) models (Table 2). For the 1,200 V/400 A model, two types of packages are provided: one is for designing compact equipment and the other is for designing when much heat will be generated due to high loads. The forms were designed such that they can be used as replacements, considering compatibility with currently-used packages.

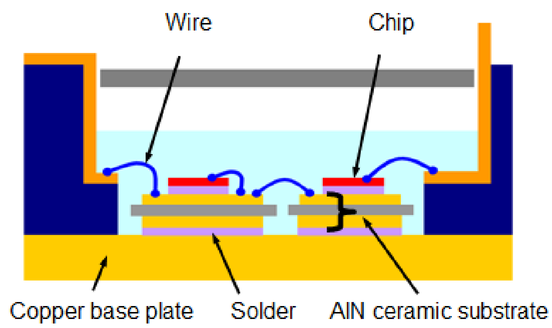

Fig. 8 Internal structure (TH-series)

Table 2 Line-up (TH-series)

V_{ces}	Topology	Package	I_c[A]		
			200	400	600
1200V	2in1	48x94mm^2 	■ CM200DY-24TH		
		62x108mm^2 		■ CM400DY-24TH	
		80x110mm^2 		■ CM400DU-24TH	■ CM600DU-24TH

3. Conclusion

This paper described the seventh-generation industrial IGBT module TH-series with the high-speed switching specification. To make equipment more efficient, it is important to reduce the loss of the power devices. However, there are many applications of industrial equipment and service conditions also vary. Accordingly, there is no single specification that can cover all power devices and improve the efficiency of all equipment. It is important to optimize the properties of power devices based on the service conditions of equipment in order to make best use of it. In recent years, to enhance the performance of equipment, wide band gap (WBG) devices can also be selected because they may work well to reduce the loss. Meanwhile, Si devices, which are reaching the upper limit to improvements to their properties, may still contribute to equipment for which they are used by adjusting the IGBT's properties. We will continue to develop products to support various service conditions and various circuit configurations of equipment in the future.

References

(1) R. Kamibaba, et al.: 7th Generation Power Chip Technologies for Industrial Applications, Mitsubishi Denki Giho, 90, No. 5, 287–290 (2016)

(2) Masaomi Miyazawa, et al.: 7th Generation IGBT Module "T Series" for Industrial Applications, Mitsubishi Denki Giho, 90, No. 5, 295–298 (2016)

The Investigation of Humidity Absorption Behavior of Silicone Gel in HVIGBT Modules

Authors: *Kenji Hatori** and *Wakana Noboru***

1. Introduction

Railway transportation is more energy-efficient than other transportation means and thus reduces the environmental impact of the entire transportation sector. Consequently, railway usage is being encouraged around the world to help combat global warming. In addition, to realize a low-carbon society, non-electrified railways are being electrified and more accumulator cars have been introduced. As a result, electric trains are now being used in various environments around the world.

Power modules for railway cars need to be small and efficient (low loss) and also more reliable than those for consumer goods and general industrial applications. Therefore, there is a growing need to evaluate resistance to diverse environments. In humid environments, in particular, it is difficult to completely eliminate the influence of humidity because modules have not been sealed. There are strong demands for higher humidity resistance and resistance evaluation technologies.

Under such circumstances, Mitsubishi Electric Corporation has worked to improve the humidity resistance of HVIGBT modules and establish humidity resistance evaluation technologies. Regarding penetration of moisture, HVIGBT modules are filled with silicone gel, which acts as a low-pass filter. Understanding the humidity absorption behavior of this silicone gel is important when assessing the humidity resistance of HVIGBT modules. However, the humidity absorption behavior at the level of the raw material (e.g., silicone gel) had not been studied. Therefore, we studied the humidity absorption behavior of silicone gel. This paper describes the results.

2. Humidity Absorption Behavior of Silicone Gel

Generally, IGBT modules are filled with silicone gel. Resin-like silicone gel absorbs moisture depending on the surrounding environment and it is known that the moisture content can be explained by the diffusion and dissolution of water vapor.[(1)(2)] The water vapor solubility (c) is expressed by a diffusion coefficient (D) using Fick's law shown as formula (1). This diffusion coefficient (D) is expressed by a frequency factor (D_0), gas constant (R), activation energy (E_D), and temperature (T) as shown in formula (2).

$$\frac{\partial c}{\partial t} = \frac{\partial}{\partial x}\left(\boldsymbol{D}\frac{\partial c}{\partial x}\right) \qquad (1)$$

$$D = D_0 \exp\left(-\frac{E_D}{RT}\right) \qquad (2)$$

Meanwhile, the solubility when the humidity absorption is sufficiently saturated ($c_{(t=\infty)}$) is expressed by a solubility coefficient (S) and vapor pressure (P_v) as shown in formula (3). This solubility coefficient (S) is expressed by a frequency factor (S_0), gas constant (R), and enthalpy (ΔH_S) as shown in formula (4).

$$c_{(t=\infty)} = S \cdot P_v \qquad (3)$$

$$S = S_0 \exp\left(-\frac{\Delta H_S}{RT}\right) \qquad (4)$$

It is important to determine the diffusion coefficient (*D*) and solubility coefficient (*S*) to understand the humidity absorption behavior of silicone gel. We therefore measured the trend of the increase in the weight of silicone gel when it absorbed moisture. As shown in Fig. 1, a metal cylinder with a radius of 2.5 mm was filled with silicone gel to a depth of 1.823 mm as a sample. Several such samples were prepared and dried at 50°C, 0%RH for eight hours. Then, one sample was put into a container at each of 25°C, 45%RH; 40°C, 45%RH; and 45°C, 45%RH and changes in the weight were measured.

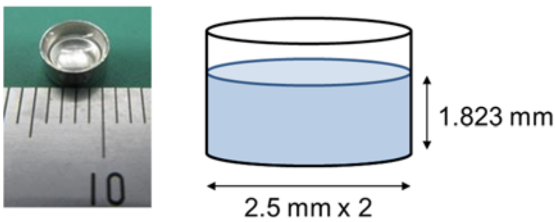

Fig. 1 Silicone gel sample for weight measurement under humidification

*Power Device Works **Advanced Technology R&D Center

Table 1 Vapor concentration at the end with various conditions

Ambient environment	Water vapor solubility of silicone gel	Vapor concentration of air
25 °C / 45%RH	2.89×10^{-4} mg/mm³	1.04×10^{-5} mg/mm³
40 °C / 45%RH	4.05×10^{-4} mg/mm³	2.30×10^{-5} mg/mm³
45 °C / 45%RH	4.39×10^{-4} mg/mm³	2.94×10^{-5} mg/mm³

Table 1 and Fig. 2 show the measurement results. As listed in Table 1, the water vapor solubility of silicone gel is approximately 20 times the vapor concentration of air. This suggests that water vapor had dissolved into the silicone gel. These results can be used to calculate the solubility (S) under each condition using formula (3). Figure 3 shows that the solubility coefficient (S) is negatively correlated with temperature. From Fig. 3 and formula (4), the calculated enthalpy (ΔH_S) is -26.8 kJ/mol and the frequency factor (S_0) is 4.12 x 10^{-12} mg/(mm³·Pa).

Meanwhile, Bryan Ellis proposed a method to calculate the diffusion coefficient (D) approximately using the gradient of the increase in the solubility;[3] formula (5) is an approximate formula, where “L” is the thickness of the sample resin. In Fig. 4, the horizontal axis is $t^{0.5}/L$ and the vertical axis is $c(t)/c_{(t=\infty)}$. The gradient of the weight increase curve was calculated in the range of $0.2 < c(t)/c_{(t=\infty)} < 0.6$. Table 2 and Fig. 5 show the results.

$$\frac{c(t)}{c_{(t=\infty)}} = 2\sqrt{\frac{Dt}{L^2\pi}} \qquad (5)$$

Figure 5 shows that the water vapor diffusion coefficient of the silicone gel is positively correlated with temperature. From Fig. 5 and formula (2), the calculated activation energy (E_D) is 20.8 kJ/mol and the frequency factor (D_0) is 40.3 mm²/s.

The solubility at 40°C, 80%RH calculated using the obtained solubility coefficient is 715 g/m³. During rapid cooling, the solubility (SH) can be regarded as constant. Accordingly, from the curve of SH = 715 g/m³ in Fig. 6, it is understood that when the temperature decreases by 10.5 K from 40°C, 80%RH, the inside of the silicone gel condenses. On the other hand, during rapid cooling, the absolute humidity (AH) of the air can be regarded as constant. From the curve of AH = 41 g/m³ in Fig. 6, it is understood that when the temperature decreases by 4.4 K from 40°C, 80%RH, condensation occurs in the air. These results show that condensation tends to not occur in the silicone gel compared to in air.

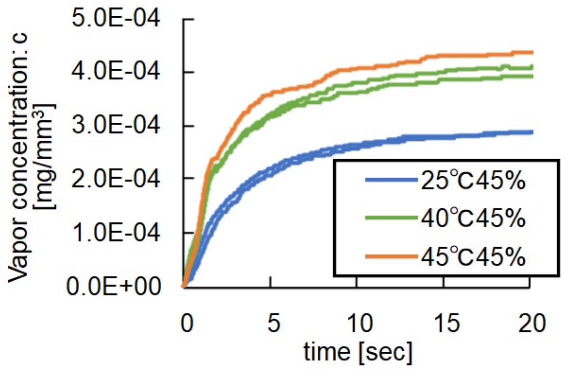

Fig. 2 Silicone gel weight increase trend with various conditions

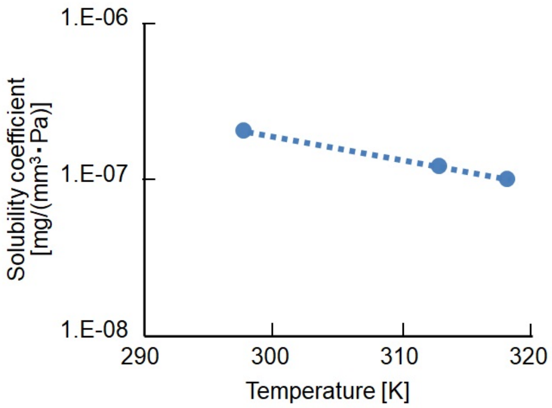

Fig. 3 Solubility coefficient temperature dependency of silicone gel

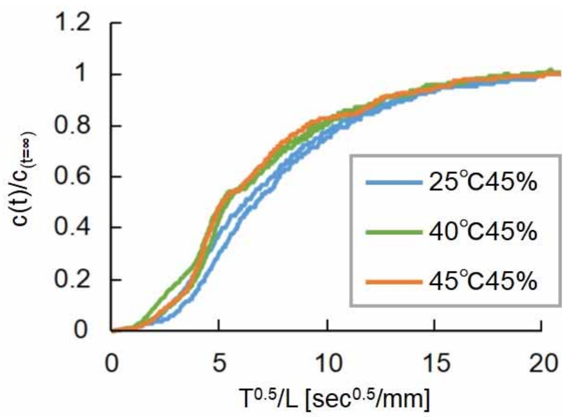

Fig. 4 Silicone gel weight increase trend with various conditions.

3. Humidity Absorption Behavior of Gel in Market Environments

The humidity absorption risk in market environments was studied using the calculated water vapor solubility coefficient and water vapor diffusion coefficient of the silicone gel. In this study, the thermal effect of devices' operation was not considered. The conditions were simplified and the temperature change due to the outside air were assumed to be the same as the temperature change of the devices. From data on environments in Tokyo and London in 2020, days on which the humidity was relatively high were selected from summer and winter and the humidity absorption by silicone gel was simulated. Figures 7 to 10 show the results.

The humidity near the chips (local humidity) tends to be higher in the early morning, which indicates that the condensation risk is the highest in the early morning. However, the results show that even when the relative humidity in the ambient environment is close to 100%, the humidity near the chips is below 100%. These simulation results also suggest that condensation tends to not occur inside modules compared to in the ambient environment.

Table 2 Diffusion coefficient of silicone gel

Ambient environment	Gradient of weight increase $2\times(D/\pi)^{0.5}$	Diffusion coefficient
25 °C/45%RH	0.108 $mm/s^{0.5}$	9.19×10^{-3} mm^2/s
40 °C/45%RH	0.135 $mm/s^{0.5}$	1.44×10^{-2} mm^2/s
45 °C/45%RH	0.137 $mm/s^{0.5}$	1.48×10^{-2} mm^2/s

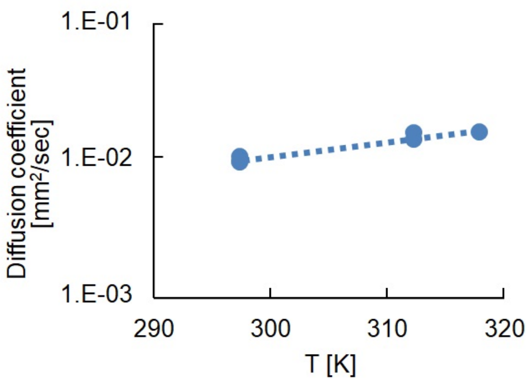

Fig. 5 Diffusion coefficient temperature dependency of silicone gel.

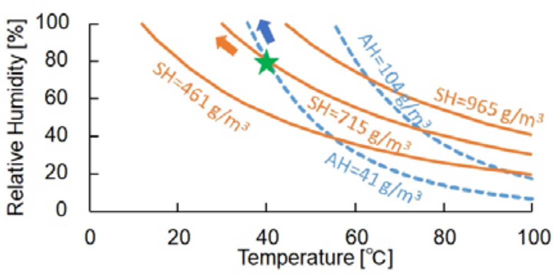

Fig. 6 Dissolved humidity (SH) & absolute humidity (AH)

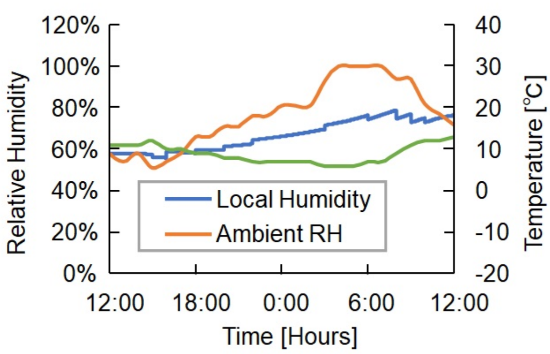

Fig. 7 Humidity absorption during day cycle in winter (1 – 2 Feb. 2020) in London.

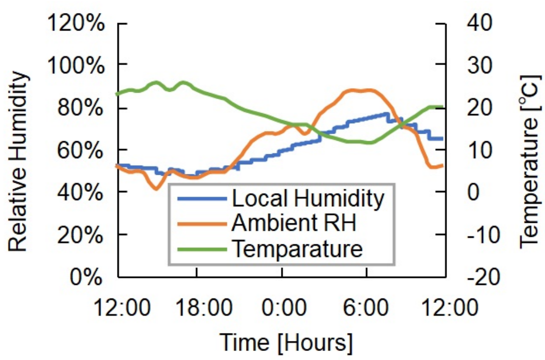

Fig. 8 Humidity absorption during day cycle in summer (1 – 2 Aug. 2020) in London.

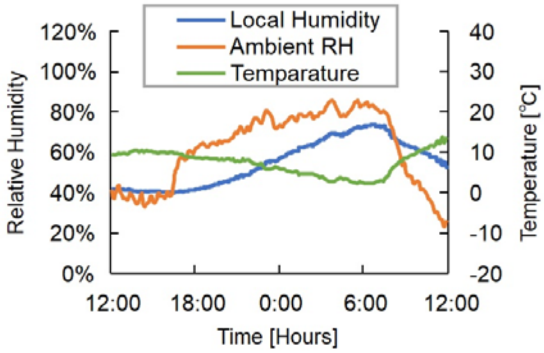

Fig. 9 Humidity absorption during day cycle in winter (4 – 5 Feb. 2020) in Tokyo.

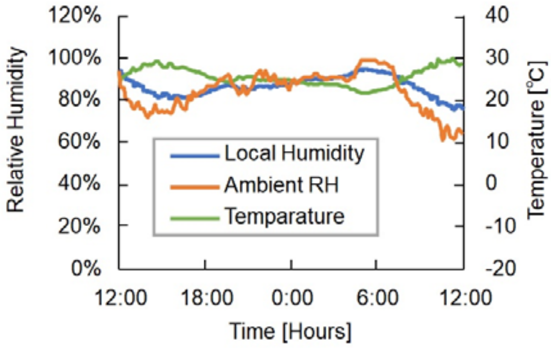

Fig. 10 Humidity absorption during day cycle in summer (31 Jul. – 1 Aug. 2020) in Tokyo.

4. Conclusion

Based on the experimental results, the water vapor solubility coefficient and water vapor diffusion coefficient of the silicone gel were calculated. The results showed that the condensation risk inside the silicone gel is smaller than in the ambient environment.

Mitsubishi Electric is using these developed humidity resistance evaluation and improvement technologies to increase the reliability of power semiconductor modules, contributing to realizing a low-carbon society and comfortable living.

References

(1) T. Mizutani: Warpage Analysis in LCD Panel under Moisture Diffusion and Hygroscopic Swelling, Journal of Japan Institute of Electronics Packaging, Vol. 12, 144-153 (2009)

(2) K. Nagai: Barrier Technology, KYORITSU SHUPPAN CO., LTD., 62-63 (2014)

(3) B. Ellis, et al.: The effects of water absorption on a polyester/ chopped strand mat laminate, Composite, 14, 237 (1983)

Built-in BSD-Function 600V High Voltage Integrated Circuit "M81777FP"

Authors: *Yo Habu** and *Shohei Sano**

1. Introduction

In recent years, there has been a growing global trend toward environmental protection such as carbon neutrality and the Sustainable Development Goals (SDGs). Power semiconductors are key parts for saving energy and raising efficiency and thus reducing environmental impact. Amid these circumstances, the use of inverters in motor drive systems for home appliances and industrial equipment has been expanding steadily. Also, there is growing demand for driver ICs that use inverter systems to drive power semiconductors. To increase the capacity of the inverter while reducing its size, the drive systems also need to contribute to downsizing and fewer parts.

As technologies for driver ICs such as our high-voltage integrated circuits (HVICs), we developed our proprietary divided RESURF structure (first generation) in 1997 and commercialized 1,200-V HVICs. In 2008, we developed and commercialized the second-generation divided RESURF structure with higher withstand voltage and larger malfunction tolerance for the 600-V class by fine-pattern forming an N+ buried layer on the first-generation divided RESURF structure.(1) In addition, we applied our proprietary field plate technology to this second-generation divided RESURF structure to increase the withstand voltage to 1,200 V and have been working to commercialize it.(2) The divided RESURF structure is applied to laterally double-diffused metal-oxide-semi-conductor field-effect-transistors (LDMOSFETs). LDMOSFETs are used to convert the voltage to a level to drive high-side circuits; this is called high-voltage level shift in HVICs. Applying the divided RESURF structure increases the withstand voltage and malfunction tolerance while remarkably reducing the area that the LDMOSFETs occupies on a chip. This makes it possible to enhance the drive performance of the driver IC per chip area (larger capacity and higher voltage) and to include protection circuits and power circuits, which used to be configured with external components, thus downsizing and reducing the number of parts and greatly enhancing the system performance.

This paper outlines the built-in BSD-function 600-V high voltage half-bridge driver M81777FP developed this time along with its key technologies, performance and quality. This M81777FP half-bridge driver has a built-in diode function for bootstrap circuits.

2. Built-in BSD-Function 600-V High Voltage Half-bridge Driver M81777FP

2.1 Product outline of M81777FP

Figure 1 shows a functional block diagram of the built-in BSD-function 600-V high voltage half-bridge driver M81777FP. Its functions are listed below.

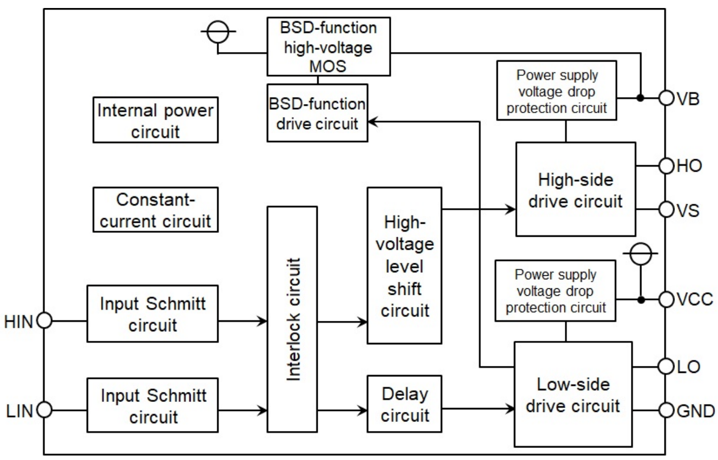

Fig. 1 Functional block diagram of M81777FP

*Power Device Works

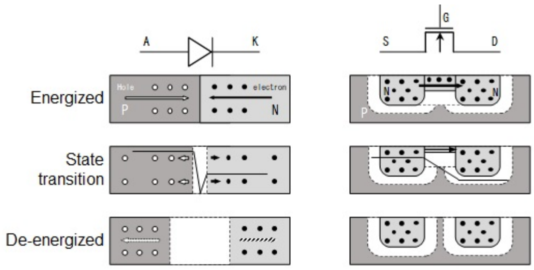

Fig. 2 Comparison of conductive state between diode and MOSFET

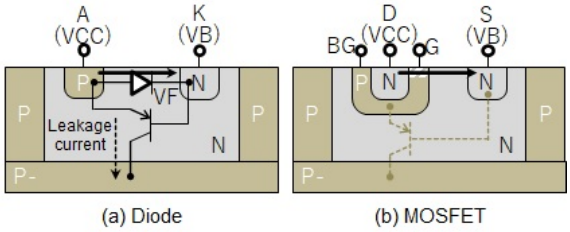

Fig. 3 Cross section of diode and MOSFET

(1) Half-bridge drive
(2) 600-V high-voltage built-in BSD-function
(3) Interface supporting 3.3- and 5.0-V logic input
(4) Input interlock (to prevent the output turning on simultaneously)
(5) 600-V high-voltage level shift circuit
(6) Output current performance (+200 mA/−350 mA)
(7) Power supply voltage drop protection circuits (UV: VCC/VBS)

To make it easy to replace the conventional basic models M81736FP and M81776FP, the M81777FP was designed with compatible pin locations and various properties other than the BSD function.(3)

2.2 Built-in diode function for bootstrap circuits

2.2.1 Use of high-voltage MOSFETs for the BSD function

On the M81777FP, the diode function necessary for bootstrap circuits is realized by operating the high-voltage MOSFETs in ICs as an alternative means. Details of the technologies that allow MOSFETs to be used for charging operation are described below along with their advantages.

(1) Suppression of recovery currents and leakage currents when energized

Figure 2 illustrates the movement of carriers in a diode and MOSFET when energized. For a diode, there are two types of carriers that generate currents: holes, and electrons, so it is a bipolar device. When the state changes from energized to de-energized, the carriers travel in the opposite direction until a depletion layer forms. The movement of carriers in this transition region results in recovery currents and surges. On the other hand, for a MOSFET, there is only one type of carrier that generates currents, so it is a unipolar device. When the state changes from energized to de-energized, no new depletion layer area is formed and whether a current is generated is determined only by the presence or absence of a channel. Accordingly, although recovery currents are problems in diodes, no such currents are generated in MOSFETs.

One advantage of charging operation by MOSFETs is that leakage currents during charge can also be suppressed. Figure 3 illustrates cross sections of a diode and MOSFET. In the diode configuration, when it is biased from the P to N direction, forward voltage VF is generated due to the PN junction. Because the IC is in a junction isolation structure, parasitic PNP Tr occurs with the substrate (P-) as a collector. As the charging current is larger, more base current for this parasitic PNP Tr is secured and the leakage current toward the substrate increases. This current loss makes it difficult to secure product quality because it sometimes causes a latchup phenomenon or other problems. On the other hand, in a MOSFET, the charging current flows from the drain (N) to the source (N) and so no forward voltage VF due to the PN junction is generated. Although parasitic PNP Tr exists in this configuration, if the bias between the MOSFET back gate and source is appropriately treated, no leakage current toward the substrate occurs. Accordingly, the MOSFET configuration is more advantageous for ensuring product quality than the diode configuration.

(2) Gate drive of BSD-function MOSs

Diodes function in a passive way whereby the bias condition of the terminals uniquely determines the state (energization and non-energization). On the other hand, MOSFETs are active elements for which the bias condition of each terminal determines energization, non-energization, amplification, and attenuation. To use MOSFETs for charging operation, the bias of the terminals-gate drive signals in particular-needs to be appropriately applied. Figure 4 shows a simplified circuit structure of a conventional bootstrap circuit consisting of external elements and that where a MOSFET inside an IC is used for charging operation.

In a bootstrap circuit, a diode and resistance are connected between the primary power source (VCC) and secondary power source (VB) and the secondary reference potential (VS) determines whether charging is performed. In the conventional structure, because a diode is connected, when potential VS decreases, charging is performed; and when it increases, the diode is reverse-biased and de-energized in due course.

On the other hand, because MOSFETs are active elements as described above, MOSFET gate drive signals need to be appropriately given to use them for this charging operation.

Figure 5 shows an inverter circuit of half-bridge drive. Whether charging is performed is determined based on potential VS (reference potential). Accordingly, the signal to determine potential VS needs to be synchronized with the BSD-function MOS gate drive signal. Potential VS is the potential at the point at which an output node of the inverter (load) is connected. In a bootstrap circuit, charging operation is performed when potential VS is low (GND level) and this is determined when the N-side transistor of the inverter is in the ON state. Consequently, when the LO output is high, the gate drive synchronization signal is given to perform charging operation and when the LO output is low, charging operation is not performed because potential VS is uncertain or high (level of the power source of the load).

(3) Securing the charging voltage of the secondary power source

The use of synchronization signals described in the previous section to drive the BSD-function MOS gate enables bootstrap charging operation. However, to charge the secondary power source such that its voltage is at the same level as that of the primary power source, the BSD-function MOS needs to be biased in a triode region. As shown in Fig. 4, which is a simplified circuit diagram of the BSD function of a high-voltage MOSFET, a boosted voltage is applied to the MOSFET gate by the charge pump circuit consisting of a diode, capacitance, and buffer circuit. Due to this, the BSD-function MOS operates as a triode and the secondary power source can be charged such that the voltage becomes the same level as that of the primary power source. Figure 6 shows the gate voltage of the BSD-function MOS for each boosting method. In the simplified circuit diagram shown in Fig. 4, boosting operation is performed once per synchronization signal and so the boosted gate potential decreases over time. For the M81777FP, in addition to the structure where boosted voltage is applied to the BSD-function MOS gate, our proprietary circuit structure is used. In the structure, while a synchronization signal is given, the boosted voltage to the gate can be retained. In this booster circuit configuration, the gate potential is kept excited by the boosting operation, which enables stable charging operation.

In addition, in the simplified circuit structure, the potential of the gate voltage is the same as that of VCC and the voltage between the MOSFET gate and source is 0 V when the BSD-function MOS is in the OFF state. Meanwhile, for the M81777FP, 0 V is given as the gate potential to make the OFF state “strong”. This bias method secures a large tolerance to momentary interruption of the primary power source and a malfunction when switching noise occurs on the inverter.

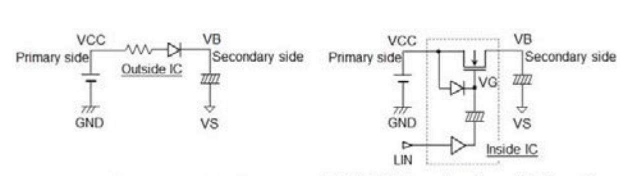

(a) Conventional bootstrap circuit (b) BSD function by a high-voltage MOSFET

Fig. 4 Simplified circuit structure of each method for charging

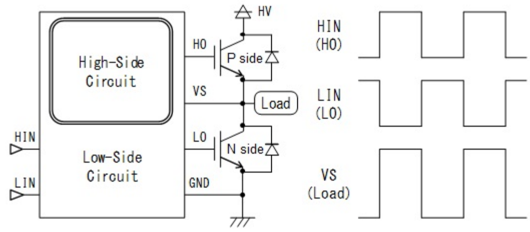

Fig. 5 Inverter circuit of half-bridge drive

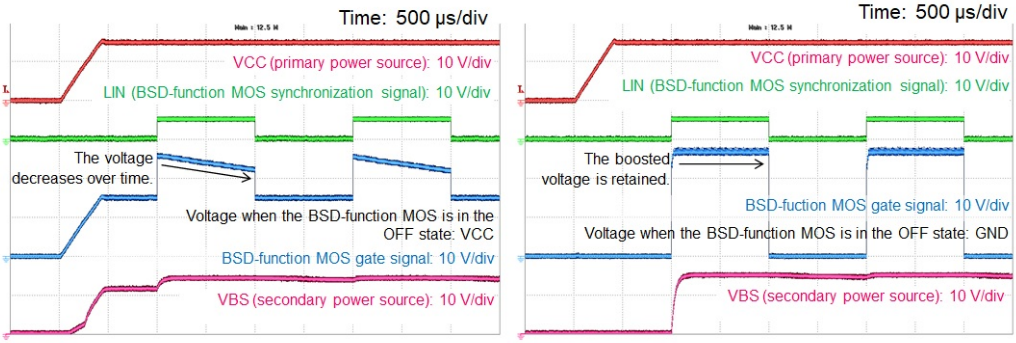

(a) Charging operation by the BSD-function MOS of the simplified circuit

(b) Charging operation by the BSD-function MOS of the M81777FP

Fig. 6 Charging function of each method for boosting using BSD-function MOS

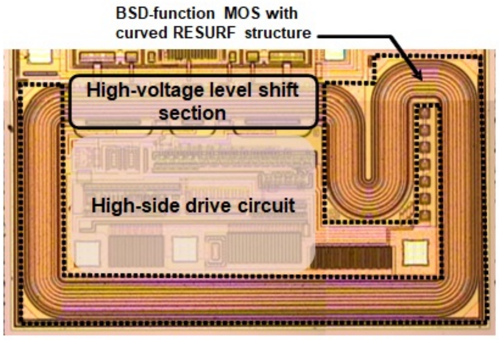

Fig. 7 BSD-function MOS layout of M81777FP

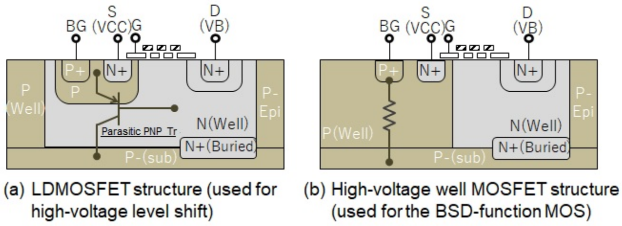

Fig. 8 Cross section of high voltage MOSFET

2.2.2 Current limiting resistance by the on-resistance of the BSD-function MOS

In addition to diodes and capacitors, another element necessary for bootstrap charging is current limiting resistance to suppress surge currents during charging. For the M81777FP, current limiting resistance is realized by the on-resistance of the BSD-function MOS. Figure 7 illustrates the layout of the M81777FP BSD-function MOS. For HVICs, LDMOSFETs are independently arranged by the divided RESURF structure for high-voltage level shift and a BSD-function MOS is provided in a different area. Because the on-resistance of the MOSFET is used as current limiting resistance, the W width of the MOS needs to be adjusted to set a resistance value. If the RESURF structure is extended to secure the W width, a dead space is formed in the high-side drive circuit area. To solve this problem, we have developed a new curved RESURF structure for the M81777FP and this makes it possible to set a current limiting resistance value while minimizing the dead space. For the M81777FP, the current limiting resistance value is adjusted to be 100Ω.

2.2.3 High-voltage MOSFET structure used for BSD-function MOSs

As high-voltage MOSFET structures, there are LDMOSFETs for high-voltage level shift as described in the previous section. For BSD-function MOSs, our newly-developed proprietary high-voltage well MOSFET structure was adopted to secure malfunction tolerance. Figure 8 illustrates the cross-sectional structure of a conventional LDMOSFET and the high-voltage well MOSFET developed this time. One difference between the high-voltage well MOSFET and LDMOSFET is that the new type of MOSFET involves deep P-well diffusion where the MOS back gate is in contact with the substrate (P-).

When an LDMOSFET used for high-voltage level shift is applied as a BSD-function MOS, the back gate and source of the MOS need to be independent and the current input from the back gate to the drain needs to be suppressed. As shown in Fig. 8, in the LDMOSFET structure, there is parasitic PNP Tr between the back gate, drain, and substrate. Generally, parasitic PNP Tr is biased in an OFF state and so does not cause malfunctions. However, during initial charging of the secondary power source (VB) or by a VS negative potential surge that occurs in freewheel diode flowback mode during inverter switching, this parasitic PNP Tr may be active. Accordingly, there were problems with securing malfunction tolerance, including an increase in leakage currents and the occurrence of latchup. For the high-voltage well MOSFET developed this time, as shown in Fig. 8, the back gate is in contact with the substrate and so there is no parasitic PNP Tr which can cause malfunctions. Thanks to this, the M81777FP has large malfunction tolerance to noise during initial charging and VS negative potential surges.

3. Conclusion

We have developed the built-in BSD-function 600-V half-bridge driver M81777FP in which the high-voltage MOSFETs in ICs provide the diode function necessary for bootstrap circuits. This will help reduce the number of parts in inverter drive systems.

References

(1) K. Shimizu, et al.: High Voltage IC Technology with 2nd Generation Divided RESURF Structure, Mitsubishi Denki Giho, 84, No.4, 228–231 (2010)
(2) Y. Habu, et al.: High Reliability 1,200V HVIC "M81738FP", Mitsubishi Denki Giho, 88, No.5, 289–292 (2014)
(3) Y. Habu, et al.: Popular Edition 600V High Voltage Integrated Circuit "M81776FP", Mitsubishi Denki Giho, 94, No.3, 189–192 (2020)

Development of SiC Trench MOSFET with Novel Structure Enabling Lower Losses

Authors: *Katsutoshi Sugawara** and *Yutaka Fukui ***

1. Introduction

Amid growing environmental awareness, the energy efficiency of power electronics equipment has been improved and SiC has been attracting attention as the next-generation power semiconductor material. Compared to conventional Si, the band gap of SiC is wider and the breakdown field is higher; moreover, SiC power devices have excellent properties. Mitsubishi Electric Corporation has been developing and mass-producing SiC-MOSFETs and SiC-SBDs and has commercialized products with a wide range of breakdown voltage classes, from 600 V for home appliances to 3.3 kV for electric railways.

To improve the energy efficiency of power electronics equipment, it is important to reduce the loss of the power devices used for such equipment. Mitsubishi Electric has been using planar-gate MOSFETs which feature low resistance. Meanwhile, for trench-gate MOSFETs, which have a structure where gate electrodes are vuried in the drift layers, the unit cell size can be reduced compared to the planar type while higher integration is expected to reduce the on resistance. However, electric fields tend to concentrate on the trench bottoms of the trench type and such electric fields need to be reduced to ensure device reliability. Previously, Mitsubishi Electric proposed a structure where a p-type protective layer (BPW) provided at the trench bottom was grounded to reduce the electric field.(1) However, as shown in Fig. 1(a), higher integration was difficult because the unit cell pitch depends on the size of BPW contact cell. To solve this problem, we developed the MIT2-MOS with a new device structure featuring an improved contact structure.

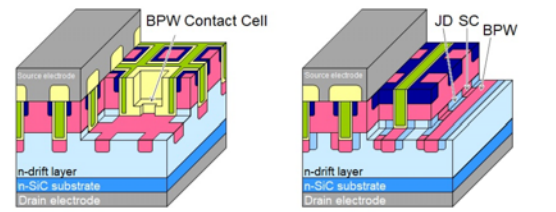

(a) Conventional structure (b) Newly developed structure (MIT2–MOS)

Fig. 1 Schematic diagrams of trench-gate MOSFET

This paper describes the structure and performance of the MIT2-MOS.

2. MIT2-MOS

2.1 Structure of the MIT2-MOS

The MIT2-MOS is characterized by three implanted layers. Figure 1(b) is a schematic diagram of the MIT2-MOS.

The first layer is a BPW at the trench bottom and this is formed by opening a trench on the SiC drift layer and implanting p-type ions from the directly facing position. This BPW alleviates a high electric field applied to the trench bottom as described in Section 1. However, the potential of floating BPW is unstable, it causes the switching loss increases. In addition, a depletion layer formed by the BPW causes narrowing of the current paths between the PW and BPW and between the BPW and BPW, increasing the resistance.

The second layer SC is provided to solve the former problem. This is formed by implanting p-type ions diagonally to the opened trench. The BPW is grounded by the SC, which stabilizes the BPW potential and reduces the switching loss.(2)

The third layer JD is provided to solve the latter problem. It is formed by implanting n-type ions diagonally to the trench. Providing an n-layer with higher ion density than the n-SiC drift layer suppresses expansion of the depletion layer from the BPW and prevents the resistance from increasing due to narrowing of the current paths.(3)

MIT2-MOSs can be manufactured by low-energy ion plantation by tilted ion implantation to the trench walls. In addition, epitaxial re-growth after ion implantation is not required and so the devices can be manufactured by simple processes. Another advantage is that higher integration is easier thanks to the simple structure.

*Advanced R&D Center **Power Device Works

2.2 Static characteristics of the MIT2-MOS

Generally, a MOSFET's threshold voltage (Vth) is in a trade-off relationship with the specific on resistance (Ron). Decreasing Vth lowers the Ron. However, a lower Vth makes it easier for a leakage current between the drain and source. In addition, Vth decreases as the temperature increases and so a high Vth is required depending on the application. Figure 2 shows the relationship between Ron and Vth. The assumed voltage class is 1.2 kV and the actual avalanche voltage is 1.5 kV. The graphs show that the increase in Ron in the high Vth region is suppressed for the trench type compared to the conventional planar type. For example, when Vth is 4.1 V, Ron is 1.9 mΩcm^2. This value is approximately half that of the planar type. Although Mitsubishi Electric reported that an increase in Ron could be suppressed in the high Vth region even for the planar type by applying re-oxidation to gate process,[4] the trench type offers superior improvement effect.

Meanwhile, the input capacitance Ciss of the trench type is larger than that of the planar type because of an increase in the channel width density. As a performance index of FOM (figure of merit) for this, the product (RonCiss) of specific on resistance and input capacitance in Fig. 3 is often used. This index for the trench type is slightly smaller than that for the planar type and the trench type's product (RonCrss) of the specific on resistance and reverse capacitance is almost the same as that of the planar type. These results show that for chips with the same Ron, the chip size of the trench type is smaller and its Ciss is also smaller.

2.3 Dynamic characteristics of the MIT2-MOS

Table 1 compares the dynamic characteristics. When comparing the planar-gate MOS and MIT2-MOS at the same dV/dt by adjusting the external gate resistance Rg, dI/dt of the trench type is larger than that of the planar type. Although this makes the turn-on loss (Eon) smaller, the turn-off loss (Eoff) of the trench type is larger. When the external gate resistance of the turn-off is changed such that dV/dt becomes equal to that of the turn-on and dV/dt and dI/dt are made larger, the sum of the trench type's Eon and Eoff is smaller than that of the planar type.

2.4 Reliability of the MIT2-MOS

As described in Section 1, the electric field at the trench bottom of the trench type tends to be larger than that of the planar type. In addition, the crystalline face on which a gate oxide forms differs between the trench type and planar type and it is known that when strong gate stress is applied to the trench type, Vth shifts.[5] Gate stress was applied to the MIT2-MOS and changes in the properties were examined. Figure 4 shows the results. When Vth was increased by 0.23 V by applying stress, the increase in Ron was approximately 2% at room temperature and only 1% or less at 150°C. This is equal to the increase in Ron when Vth increased by 0.23 V in the relationship between Ron and Vth shown in Fig. 2. This reveals that the increase in Ron is caused only by the increase in Vth and that Ron itself is not increased by the application of stress. The switching loss also shifts in line with the increase in Vth and the sum of Eon and Eoff before the stress was applied is the same as that after the stress was applied.

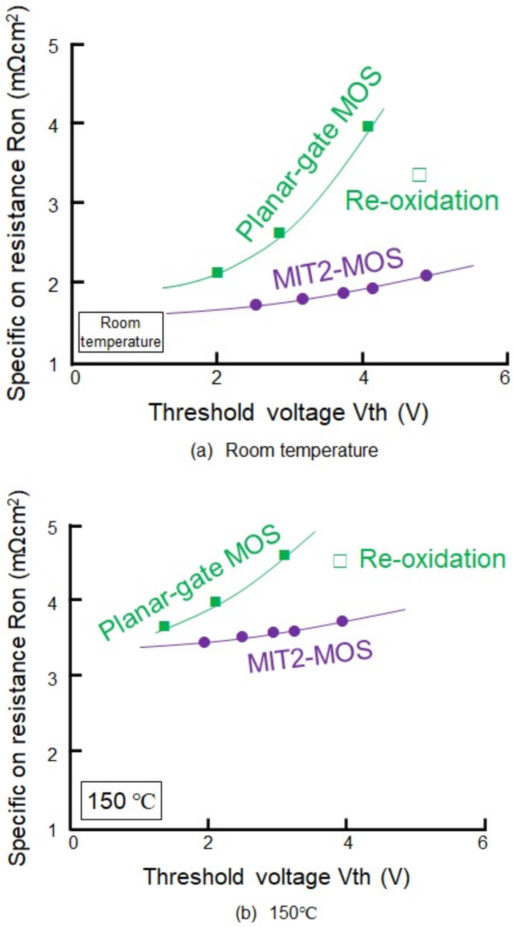

Fig. 2 Relationships between Ron and Vth for planer-gate MOSFET and MIT2-MOS at (a) R.T. and (b) 150 °C.

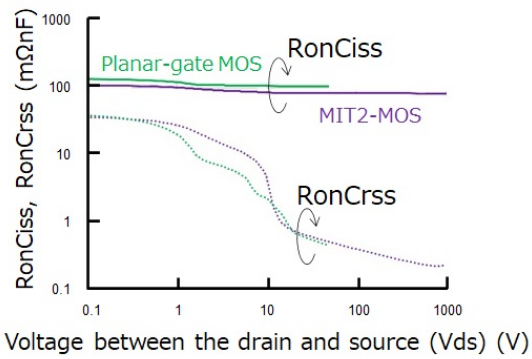

Fig. 3 Vds dependences of RonCiss and RonCrss

Vth shift may be caused by changes in the state of the gate oxide. To confirm this, two devices after stress was applied were subjected to a high-temperature reverse bias (HTRB) test. Figure 5 shows the changes in Vth measured during the test. As the stress was applied for a longer time, Vth decreased and after 200 hours, Vth hardly changed. The Vth shift amount when the application of stress began was 0.23 V, and had reduced by 0.20 V after 200 hours had passed, but then changed little up to 1,000 hours. These results show that 0.20 V among the shift amount of 0.23 V is a temporary shift and it changes based on the stress applied to the device. In addition, as a result of a 1,000-hour HTRB test, the increase in Ron and leakage current is limited to 5% or less. These results show that even devices for which Vth shift has occurred are not degraded by a HTRB test.

Table 1 Comparison of SW characteristics in planar-gate MOS and MIT2-MOS

		Planar-gate MOS	MIT2–MOS		
Threshold voltage Vth	V	1.8	3.7		
Turn-On					
Rg*1			A	B	A
dV/dt	kV/μs	8.0	8.0	6.0	8.0
dI/dt	kA/μs	1.8	2.1	1.78	2.1
Eon	mJ/P	1.1	0.8	1.8	0.8
Turn-Off					
Rg			B	B	A
dV/dt	kV/μs	10.0	10.0	10.0	15.0
dI/dt	kA/μs	0.9	1.1	1.1	2.6
Eoff	mJ/P	2.1	2.7	2.7	2.0
Eon + Eoff	mJ/P	3.2	3.5	4.5	2.8
vs planar type	%		+10.9	+40.6	-12.5

Note 1: Rg refers to the external gate resistance of the MOSFET.

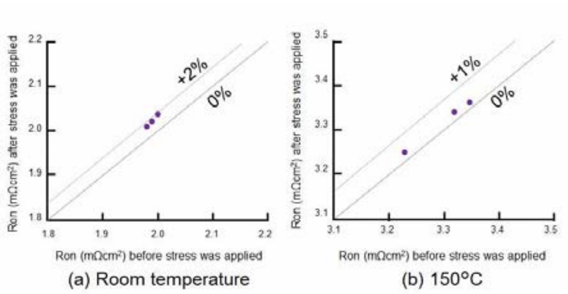

Fig. 4 Changes of Ron after gate stress at (a) R.T. and (b) 150 °C.

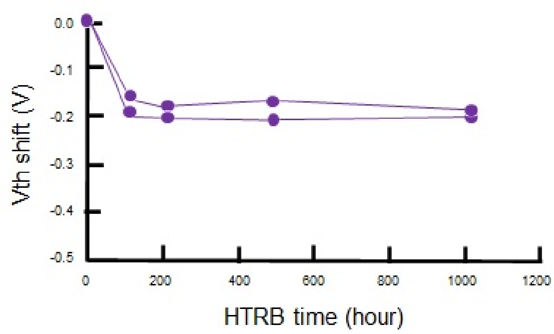

Fig. 5 HTRB stabilities of Vth after gate stress

3. Conclusion

We have developed MIT2-MOSs that include BPWs which alleviate the electric fields applied to trench bottoms, SCs that ground the BPWs, and JDs that prevent narrowing of current paths. The rating of the developed 1.2 kV class MIT2-MOS (avalanche voltage of 1.5 kV), the threshold voltage is 4.1 V, and the specific on resistance is 1.9 mΩcm^2. This latter value is approximately half that of the planar type which is being commercialized. In addition, a large stress was applied to the gate to cause Vth shift of 0.23 V and the influence on the static characteristics, dynamic characteristics, and HTRB reliability was examined. The results showed no significant problems. Furthermore, 0.20 V among the Vth shift of 0.23 V was found to be a temporary shift. Thus, we have confirmed that the developed MIT2-MOS has excellent performance. We will continue to work toward mass-producing it.

References

(1) Y. Kagawa, et al.: 4H-SiC Trench MOSFET with Bottom Oxide Protection, Mater. Sci. Forum 778, 919-922 (2014)
(2) Y. Fukui, et al.: Effects of Grounding Bottom Oxide Protection Layer in Trench-Gate SiC-MOSFET by Tilted Al Implantation, Mater. Sci. Forum 1004, 764-769 (2020)
(3) R. Tanaka, et al.: Performance Improvement of Trench-Gate SiC MOSFETs by Localized High-Concentration N-Type Ion Implantation, Mater. Sci. Forum 1004, 770-775 (2020)
(4) T. Tanioka, et al.: High Performance 4H-SiC MOSFETs with Optimum Design of Active Cell and Re-Oxidation, PCIM Europe 2018, 879-884 (2018)
(5) Peters, D., et al.: Investigation of threshold voltage stability of SiC MOSFETs, Proc. of 30th ISPSD, 40-43 (2018)

MITSUBISHI ELECTRIC CORPORATION